methods

# A new, long-wavelength borondipyrromethene sphingosine for studying sphingolipid dynamics in live cells[S]

**Raehyun Kim,[1] Kaiyan Lou,[1,2] and Mary L. Kraft[3]**

Department of Chemical and Biomolecular Engineering, University of Illinois at Urbana-Champaign, Urbana, IL 61801

**Abstract** **Sphingolipids function as cell membrane components and as signaling molecules that regulate critical cellular processes. To study unacylated and acylated sphingolipids in cells with fluorescence microscopy, the fluorophore in the analog must be located within the sphingoid backbone and not the *N*-acyl fatty acid side chain. Although such fluorescent sphingosine analogs have been reported, they either require UV excitation or their emission overlaps with that of the most common protein label, green fluorescent protein (GFP). We report the synthesis and use of a new fluorescent sphingolipid analog, borondipyrromethene (BODIPY) 540 sphingosine, which has an excitation maximum at 540 nm and emission that permits its visualization in parallel with GFP. Mammalian cells readily metabolized BODIPY 540 sphingosine to more complex fluorescent sphingolipids, and subsequently degraded these fluorescent sphingolipids via the native sphingolipid catabolism pathway. Visualization of BODIPY 540 fluorescence in parallel with GFP-labeled organelle-specific proteins showed the BODIPY 540 sphingosine metabolites were transported through the secretory pathway and were transiently located within lysosomes, mitochondria, and the nucleus. The reported method for using BODIPY 540 sphingosine to visualize sphingolipids in parallel with GFP-labeled proteins within living cells may permit new insight into sphingolipid transport, metabolism, and signaling.**—Kim, R., K. Lou, and M. L. Kraft. **A new long wavelength borondipyrromethene sphingosine for studying sphingolipid dynamics in live cells.** ***J. Lipid Res.*** **2013.** 54: **265–275.**

**Supplementary key words** metabolic labeling • fluorescent sphingolipid • fluorescent sphingosine • live cell imaging • fluorescence microscopy • lipid transport • sphingolipid metabolism • sphingolipid catabolism

Sphingolipids and their metabolites serve as structural components in eukaryotic cell membranes and as bioactive signaling molecules that modulate gene expression, apoptosis, and other critical cellular processes during normal cell function and disease (1–4). Insight into sphingolipid biosynthesis, transport, and subcellular distribution has been acquired by observing fluorescent sphingolipid analogs within living cells (5). Sphingolipid derivatives that contain a fluorophore-labeled *N*-acyl fatty acid are often used to investigate dynamic processes that involve acylated sphingolipids (5). Fatty acids that contain a polyene fluorophore are especially attractive for this purpose because the structure and behavior of polyene-containing lipids are very similar to the native lipid (6). However, to study the bioactive, unacylated sphingolipids, sphingosine and sphingosine-1-phosphate, the fluorophore must be incorporated into the sphingosine backbone. Studies have confirmed that such fluorescent sphingosine analogs can be metabolized to more complex fluorescently labeled sphingolipids in living cells (7–10). Despite their potential utility, only a limited number of fluorophores, such as pyrene, borondipyrromethene (BODIPY), and nitrobenzo-2-oxa-1,3-diazole, have been incorporated into the sphingosine backbone (7–9).

To increase the utility of fluorescent sphingosine analogs for investigating sphingolipid dynamics in living cells, derivatives with a wider range of fluorescence properties must be developed. Lacking in particular is a bioactive fluorescent sphingosine that has neither an excitation maximum that is in the UV range nor emission that interferes with detecting green fluorescent protein (GFP), the most common genetically encoded fluorescent protein label (11). A probe with these properties is expected to

*M.L.K. holds a Career Award at the Scientific Interface from the Burroughs Wellcome Fund. This material is based upon work supported by the National Science Foundation under CHE–1058809.*

*Manuscript received 6 June 2012 and in revised form 22 October 2012.*

*Published, JLR Papers in Press, November 4, 2012*
*DOI 10.1194/jlr.D029207*



Abbreviations: GFP, green fluorescent protein; BODIPY, borondipyrromethene; rt, room temperature; ER, endoplasmic reticulum.

[1] R. Kim and K. Lou contributed equally to this work.

[2] Present address of K. Lou: School of Pharmacy, East China University of Science and Technology, P.O. Box 268, 130 Meilong Road, Shanghai, China, 200237

[3] To whom correspondence should be addressed.
e-mail: mlkraft@illinois.edu

[S] The online version of this article (available at http://www.jlr.org) contains supplementary data in the form of supplementary methods and figures.

have the advantages of lower phototoxicity than existing fluorescent sphingosine analogs and the capability to visualize it in parallel with GFP, which would facilitate assessing sphingolipid colocalization with proteins of interest. For this reason, here we report the synthesis and validation of BODIPY 540 sphingosine (**I**), which has maximum excitation at 540 nm and emission that does not overlap with GFP. In this study, we use fluorescent organelle-specific markers to characterize the distribution of BODIPY 540 sphingosine and its fluorescent metabolites within living cells. We confirm that mammalian cells metabolized BODIPY 540 sphingosine to BODIPY 540 sphingolipids and catabolized these fluorescent sphingolipid metabolites. On the basis of these results, we anticipate that this new fluorescent sphingosine analog will be a valuable tool for investigating the metabolism, trafficking, and signaling of acylated and unacylated sphingolipid species in living cells.

## MATERIALS AND METHODS

### Synthesis of BODIPY 540 sphingosine

All solvents and commercially available reagents were used without further purification unless otherwise stated. Tetrahydrofuran was distilled from sodium/benzophenone and dichloromethane from calcium hydride under argon. Air- and moisture-sensitive reactions were carried out in oven-dried or flame-dried glassware that was septum-capped and maintained under argon at atmospheric pressure. Flash chromatography was performed with silica gel 60, 230–400 mesh from Silicycle. Proton ($^{1}$H) and carbon ($^{13}$C) NMR spectra were recorded on 400 or 500 MHz Varian Unity instruments. ESI-HRMS was carried out on a FTICR instrument. NMR and mass spectrometry data for the compounds described below are provided in the supplementary information.

### 1-Bromo-4-(dodec-11-en-1-yloxy)benzene (II)

Under an argon atmosphere, a mixture of 4-bromophenol (1.00 g; 5.78 mmol), 12-bromododec-1-ene (1.43 g; 5.78 mmol), and potassium carbonate (1.20 g; 8.68 mmol) was refluxed in 20 ml acetone for 24 h. The reaction mixture was cooled to room temperature (rt) and filtered. The filtrate was concentrated in vacuo, and the residue was purified by flash chromatography on silica gel, eluting with hexane, affording **II** as a colorless oil (1.60 g; 82% yield).

### (4-(Dodec-11-en-1-yloxy)phenyl)boronic acid (III)

Under an argon atmosphere, *n*-butyllithium (1.6 M in hexane; 2.5 ml) was added over 5 min to 1-bromo-4-(dodec-11-en-1-yloxy)benzene (**II**) (1.12 g; 3.3 mmol) in dry tetrahydrofuran (10 ml) at −78°C (dry ice/acetone bath). The mixture was stirred at −78°C for 1 h, trimethyl borate (0.55 ml, 4.9 mmol) in dry THF (3.5 ml) was added at −78°C, and the reaction mixture was stirred for 2 h while warming to rt. Water (20 ml) was added to the reaction, and the solution was stirred for 1 h at rt. The mixture was extracted with diethyl ether (2 × 100 ml). The combined organic layer was washed with 1 M HCl (150 ml), concentrated sodium bicarbonate (aq, 150 ml), and brine (150 ml). The organic layer was dried with anhydrous magnesium sulfate, filtered, and concentrated in vacuo. The residue was purified by flash column chromatography on silica gel using hexane-ethyl acetate (1:1 v/v) as eluent, yielding **III** as a white solid (612 mg; 61% yield).

### *tert*-butyl 2-(4-(dodec-11-en-1-yloxy)phenyl)-1H-pyrrole-1-carboxylate (V)

To a suspension of tetrakis(triphenylphosphine)palladium (0) (24 mg; 0.02 mmol) and (4-(dodec-11-en-1-yloxy)phenyl) boronic acid (**III**) (310 mg; 1.02 mmol) in methanol (1.2 ml) was added *N*-boc-2-bromopyrrole (**IV**) (300 mg; 1.22 mmol) in toluene (6.0 ml) and sodium carbonate (2.0 M; 1.0 ml) under argon. The reaction mixture was refluxed for 14 h and cooled to rt, and the solvent was removed in vacuo. The residue was extracted with diethyl ether (2 × 150 ml). The combined organic layer was washed with 1 M HCl (150 ml), concentrated sodium bicarbonate (aq, 150 ml), and brine (150 ml) and then dried with anhydrous magnesium sulfate, filtered, and concentrated via rotary evaporation. The residue was purified by flash column chromatography on silica gel using a gradient of hexane and methylene chloride to afford **V** as a colorless oil (363 mg; 84% yield).

### 2-(4-(dodec-11-en-1-yloxy)phenyl)-1H-pyrrole (VI)

A solution of *tert*-butyl 2-(4-(dodec-11-en-1-yloxy)phenyl)-1H-pyrrole-1-carboxylate (**V**) (550 mg; 1.29 mmol) and sodium methoxide (350 mg; 6.48 mmol) in methanol (15 ml) was refluxed for 8 h. The solvent was removed via rotary evaporation, and the residue was extracted with chloroform (200 ml). The organic layer was washed by concentrated sodium carbonate (aq) (150 ml) and brine (150 ml) and dried over anhydrous sodium sulfate, filtered, and concentrated via rotary evaporation. The residue was purified by flash column chromatography on silica gel using a gradient of hexane and ethyl ether to afford **VI** as a pale yellow oil (383 mg; 91% yield).

### 2-((3,5-dimethyl-2H-pyrrol-2-ylidene)methyl)-5-(4-(dodec-11-en-1-yloxy)phenyl)-1H-pyrrole (VIII)

Hydrobromic acid (48%; 200 µl) was added to a mixture of 2-(4-(dodec-11-en-1-yloxy)phenyl)-1H-pyrrole (**VI**) (383 mg; 1.18 mmol) and 2,4-dimethylpyrrole-5-carboxaldehyde (**VII**) (145 mg; 1.18 mmol, synthesized in 85% yield following the reported procedure) (12) in ethanol (15 ml) at 0°C. The mixture was stirred at rt for 4 h, and the solvent was removed via rotary evaporation. The residue was extracted with diethyl ether (2 × 150 ml), and the combined organic layer was washed with saturated sodium carbonate (aq) (150 ml) and brine (150 ml). The organic solution was dried over anhydrous sodium sulfate, filtered, and concentrated to afford crude **VIII** as a brown solid (508 mg, nearly quantitative yield) that was used in the next step without further purification.

### 4,4-Difluoro-1,3-dimethyl-5-(4-(dodec-11-en-1-yloxy) phenyl)-4-bora-3a,4a-diaza-*s*-indacene (IX)

Dipyrromethene (**VIII**) (508 mg; 1.18 mmol) and 1,8-diazabicycloundec-7-ene (533 µl; 3.57 mmol) were dissolved in dry toluene (20 ml), and $BF_3{\cdot}OEt_2$ (740 µl; 6.00 mmol) was added dropwise. The mixture was heated to 90°C and stirred for 30 min. After cooling to rt, the reaction was quenched with water and extracted with diethyl ether (2 × 200 ml). The combined organic layer was washed with saturated ammonium chloride (aq) and brine and dried over anhydrous magnesium sulfate, filtered, and concentrated via rotary evaporation. The residue was purified by flash column chromatography on silica gel using hexane-methylene chloride (1:1 v/v) as eluent to afford **IX** as a red solid (460 mg; 81% yield).

**(*S*)-4-((*R*,*E*)-1-hydroxy-13-[4-(4,4-difluoro-5,7-dimethyl-4-bora-3a,4a-diaza-*s*-indacen-3-yl)-phenoxy]tridec-2-en-1-yl)-2,2-dimethyloxazolidine-3-carboxylic acid tert-butyl ester (XI)**

The Garner-allylic alcohol (**X**) (27 mg; 0.10 mmol, synthesized as reported Ref. 13 in 40% yield after purification by silica gel column chromatography using hexane-ethyl actate [8:1 v/v] as eluent) and alkenyl BODIPY 540 (**IX**) (19 mg; 0.040 mmol) were dissolved in dry methylene chloride (2 ml), and the solution was degassed. Under argon atmosphere, a catalytic amount of second generation Grubbs' catalyst (5 mg; 0.0059 mmol) was added, and the reaction mixture was refluxed for 4 h. The solvent was removed via rotary evaporation, and the crude material was purified by flash column chromatography on silica gel using a gradient of hexane and ethyl acetate as eluent to afford **XI** as a dark red solid (20 mg; 71% yield).

**(*E*)-(2*S*,3*R*)-2-Amino-15-[4-(4,4-difluoro-5,7-dimethyl-4-bora-3a,4a-diaza-*s*-indacen-3-yl)-phenoxy]pentadec-4-ene-1,3-diol (I)**

Under an argon atmosphere, protected BODIPY-sphingosine (**XI**) (20 mg; 0.028 mmol) was dissolved in 4 M HCl in dioxane (2 ml) and stirred at rt for 20 min. The solvent was removed in vacuo, and the residue was purified by flash column chromatography on silica gel eluting with chloroform-methanol-ammonium hydroxide (40:10:1 v/v/v) to afford the title compound (**I**) as a dark red solid (6 mg; 37% yield).

### Synthesis of BODIPY 540 ceramide and BODIPY 540 sphingomyelin standards

BODIPY 540 ceramide and sphingomyelin standards for TLC were synthesized by cross metathesis reaction between 4,4-difluoro-1,3-dimethyl-5-(4-(dodec-11-en-1-yloxy)phenyl)-4-bora-3a,4a-diaza-s-indacene (**IX**) and ceramide (Sigma-Aldrich) or sphingomyelin (Sigma-Aldrich), respectively, as previously reported (14).

### Cell culture

NIH3T3 fibroblast cells were grown in DMEM with 10% calf serum and 1% penicillin/streptomycin in a 5% $CO_2$ incubator at 37°C. For colocalization studies, organelle-specific fluorescent fusion proteins were expressed in HEK293 cells due to their ease of transfection. HEK293 cells were grown in DMEM with 10% FBS and 1% penicillin/streptomycin in a 5% $CO_2$ incubator at 37°C. For microscopy experiments, cells were cultured in 35 mm glass bottom dishes (MatTek, Ashland, MA) or 35 mm plastic dishes for high-end microscopy (ibidi GmbH, München, Germany). For all other experiments, cells were grown in 150 mm cell culture dishes.

### Pulse-chase labeling

Cells were incubated with BODIPY 540 sphingosine in OptiMEM supplemented with 2% calf serum (NIH3T3 cells) or 2% FBS (HEK293 cells). BODIPY 540 sphingosine was dissolved in ethanol and added to the labeling medium such that the final concentration of BODIPY 540 sphingosine was 1 or 1.25 μM. For pulse labeling, cells were incubated in labeling medium that contained 1 or 1.25 μM of BODIPY 540 sphingosine for 30 min. After labeling, the medium was removed, and the cells were washed with PBS and cultured in unlabeled growth medium for the specified chase time. For studies of BODIPY 540 sphingosine metabolism, cells were incubated in growth medium that contained 1 μM of BODIPY 540 sphingosine for the specified time.

### Lipid extraction

Cells were harvested when they reached 90% to 100% confluence. Cells were washed with cold PBS, removed from the dish with a scraper, and pelleted by centrifugation. Lipids were extracted using the Bligh and Dyer method (15). The glycolipids were selectively hydrolyzed by alkaline treatment with sodium hydroxide; this treatment did not hydrolyze the sphingolipids.

### TLC

Lipids extracts were dissolved in chloroform-methanol (20 μl; 2:1 v/v), spotted on TLC plates (Silica 60 F254 plates, EMD Chemicals), and developed in a TLC chamber using butanol-acetic acid-water (4.5:1:1 v/v/v) as the solvent. Digital imaging of the TLC plates was performed on a Typhoon 9400 imager (GE Healthcare) using 532 nm laser excitation and a 580 nm emission filter to detect the fluorescent spots. Unlabeled lipids were visualized by iodine staining. The BODIPY 540-labeled sphingomyelin, ceramide, and sphingosine were identified by their comigration with BODIPY 540-labeled sphingolipid standards. Because this solvent system primarily separated the lipid species according to their head groups, which was confirmed by the comigration of the BODIPY 540-labeled sphingomyelin and ceramide with unlabeled sphingomyelin and ceramide, respectively, in this solvent system, the remaining fluorescent lipid species were identified according to their comigration with unlabeled lipid standards.

### Glycerolipid quantification

For each labeling interval (2 h, 1 day), the total lipid extract obtained from a single labeling experiment was dissolved in chloroform-methanol (2:1 v/v) and divided into two equal portions. One portion of the total lipid extract was subjected to alkaline hydrolysis to remove the glycerolipids; the resulting fraction is referred to as the sphingolipid extract because it contained primarily sphingolipid species. For each labeling time, the total lipid extract and corresponding sphingolipid extract were applied to a TLC plate and separated using butanol-acetic acid-water (4.5:1:1 v/v/v) as the solvent system. For each labeling interval, the amount of BODIPY 540-labeled phosphoglycerolipids on the TLC plate was assessed by visualizing the spots with a Typhoon 9400 imager (GE Healthcare) using 532 nm laser excitation and a 580 nm emission filter and quantifying their fluorescence intensities. To quantify the fraction of the fluorescence that corresponded to glycerolipids, the sum of the fluorescence intensities measured for each spot that corresponded to fluorescent phosphatidylcholine, phosphatidylethanolamine, phosphatidylserine, and phosphatidylinositol was measured using ImageQuant software (GE Healthcare) and divided by the total fluorescence intensities of all of the fluorescent lipid species.

### Labeling organelles for colocalization study

For labeling the endoplasmic reticulum (ER), Golgi apparatus, and mitochondria, organelle-specific GFP protein constructs were used. For ER labeling, HEK293 cells were transfected with pAc-GFPC1-Sec61β (Addgene plasmid 15108) (16) using TransPass D2 transfection reagent (New England BioLabs, Ipswich, MA). For Golgi apparatus and mitochondria labeling, CellLight™ Golgi-GFP and CellLight™ Mitochondria-GFP (Molecular Probes), respectively, were used according to the manufacturer's protocol. One to two days after transduction, the HEK293 cells were incubated with 1 μM of BODIPY 540 sphingosine for 30 min, followed by a chase in unlabeled medium for approximately 1 day. To label the lysosomes, NIH3T3 cells were incubated with OptiMEM containing 2 mg/ml of FITC-dextran (MW 10,000; Sigma-Aldrich) for 30 min. The cells were then cultured for 5 h in unlabeled medium, followed by 30 min in medium that contained 1 μM of BODIPY 540 sphingosine and finally in unlabeled medium for a 30 min or 16 h chase. To label the nucleus,

2 μl of Hoechest 33342 (Invitrogen) stock solution (10 mg/ml) was added to the growth medium in which the NIH3T3 cells were cultured. After 30 min, the medium was replaced with unlabeled medium. After 30 min, the cells were incubated in medium with 1 μM of BODIPY 540 sphingosine for 30 min and transferred to unlabeled medium for a 2 day chase.

### Confocal laser scanning microscopy

Labeled cells were transferred to phenol red-free OptiMEM supplemented with 2% calf serum (NIH3T3 cells) or 2% FBS (HEK293 cells). The labeled cells were observed on a Carl Zeiss LSM 700 confocal microscope with 63 × 1.4 NA oil immersion objective lens at rt using a 555 nm laser to excite BODIPY 540, a 488 nm laser to excite GFP and FITC, and a 405 nm laser to excite Hoechst 33342.

## RESULTS

### Synthesis and characterization of BODIPY 540 sphingosine

Our strategy for synthesizing BODIPY 540 sphingosine (**I**) was based on the route developed by Peters et al., which used a cross-metathesis reaction to form the double bond in the sphingosine backbone (**Scheme 1**) (8). Here, the building blocks for the cross metathesis reaction were the allylic garner aldehyde (**X**) and ω-alkenyl-substituted fluorophore (**IX**). We used BODIPY TMR as the fluorophore due to its desirable fluorescence properties (ex/em ~543/569 nm and high quantum yield) and nonpolar nature (17, 18). However, for synthetic efficiency, we replaced the phenolic methyl group in BODIPY TMR with the alkyl tail of sphingosine. Our strategy for synthesizing the ω-alkenyl-substituted fluorophore (**IX**) involved condensing 2-(4-(ω-alkenyloxy)phenyl)pyrrole (**VI**) and 3,5-dimethylpyrrole-2-carboxaldehyde (**VII**) and then inserting the $BF_2$ bridge (8).

Synthesis of ω-alkenyl-substituted fluorophore **IX** began with ω-alkenylation of 4-bromophenol with 12-bromododec-1-ene. This condensation reaction produced 1-bromo-4-(ω-alkenyloxy)benzene (**II**), which was converted to the boronic acid (**III**) (19). Miyaura-Suzuki cross-coupling of the boronic acid (**III**) with *N*-Boc-2-bromopyrrole (**IV**) in the presence of $(Ph_3P)_4Pd$ and $Na_2CO_3$ gave Boc-protected 2-(4-(ω-alkenyloxy)phenyl)pyrrole (**V**) (20). Deprotection of **V** afforded 2-(4-(ω-alkenyloxy)phenyl)pyrrole (**VI**), a key building block in the synthesis of the longer wavelength BODIPY fluorophore. To complete fluorophore construction, 3,5-dimethylpyrrole-2-carboxaldehyde (**VII**) was synthesized in 85% yield following the previously reported procedure (12) and condensed with pyrrole building block **VI** to form **VIII**. Treatment of **VIII** with borontrifluoride and 1,8-diazabicycloundec-7-ene produced the ω-alkenyl BODIPY 540 fluorophore (**IX**) in 81% yield.

Synthesis was completed by cross-metathesis reaction (8) of the ω-alkenyl BODIPY 540 fluorophore (**IX**) with the Garner-allylic alcohol (**X**) that was derived from the Garner aldehyde (13) and purifed by silica gel column chromatography using hexane-ethyl actate (8:1 v/v) as eluent in 40% yield. This reaction produced the protected BODIPY 540 sphingosine (**XI**) in 71% yield. Deprotection of **XI** afforded BODIPY 540 sphingosine (**I**) in 37% yield after purification.

Characterization of the absorption and fluorescence of BODIPY 540 sphingosine in ethanol (1 μM) demonstrated that its absorption and fluorescence emission maxima were 540 and 568 nm, respectively (**Fig. 1**). Thus, the excitation and emission properties of the analog are similar to BODIPY TMR despite replacing the phenoxy methyl in BODIPY TMR with a sphingosine moiety. The long wavelength emission that is indicative of dimer formation appeared to be negligible in labeled cells.

### Cells uptake and metabolize BODIPY 540 sphingosine

We first confirmed that BODIPY 540 sphingosine was internalized by cells and metabolized to more complex fluorescent sphingolipids. Mouse fibroblast cells (NIH3T3) were pulse labeled by incubation with 1.25 μM of BODIPY 540 sphingosine for 30 min at 37°C and transferred to unlabeled medium at 37°C for various chase times before imaging at room temperature. No adverse effect on cell viability was observed during or after labeling. **Fig. 2** shows that the pulse-labeled cells exhibited strong fluorescence, confirming they internalized the BODIPY 540 sphingosine. After a 30 min chase in unlabeled medium, fluorescent tubule-like structures and vesicles of various sizes were observed inside the NIH3T3 cells (Fig. 2A). The edges of these cells did not exhibit strong fluorescence, which indicates that the plasma membrane contained low levels of fluorescent lipid species (Fig. 2A). Fluorescent vesicles were also observed in NIH3T3 cells when the duration of the chase in unlabeled medium increased to 20 h (Fig. 2B). Although the plasma membrane still appeared to be dim relative to the highly fluorescent intracellular vesicles, which were especially abundant in NIH3T3 cells, the clearer fluorescent outline of the cell's perimeter indicates that BODIPY 540 lipid species had incorporated into the plasma membrane (Fig. 2B). Overall, these observations suggest that the BODIPY 540 sphingosine was metabolized to fluorescent sphingolipids, which were transported to the plasma membrane.

To verify that the fluorescent sphingosine was metabolized fluorescent sphingolipids, NIH3T3 cells were cultured in the presence of 1 μM of BODIPY 540 sphingosine for various time intervals, and their lipids were extracted. The glycerolipids in each total lipid extract were removed by base hydrolysis (21), and the resulting fraction, referred to as the sphingolipid extract because it primarily contained sphingolipids, was separated by TLC. The BODIPY 540-labeled sphingolipids on the TLC plate could be detected with high sensitivity according to their fluorescence. Four fluorescent sphingolipid species, which included BODIPY 540 sphingosine, were detected after a labeling time as short as 2 h (Fig. 2C). Comigration with BODIPY 540-labeled sphingolipid standards confirmed that the NIH3T3 cells metabolized the fluorescent sphingosine to BODIPY 540-labeled ceramide and sphingomyelin. Because the BODIPY 540-labeled ceramide and sphingomyelin

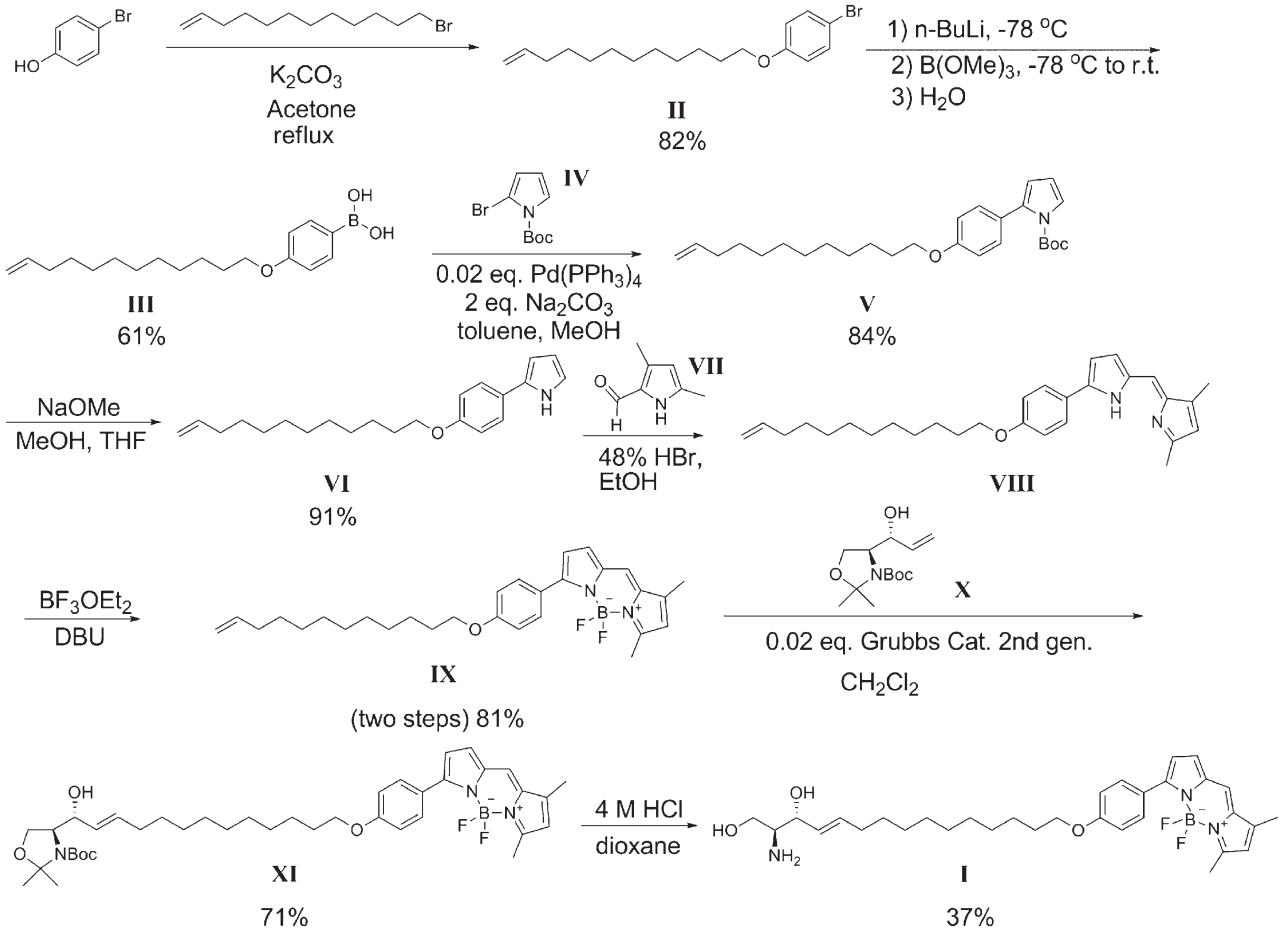


**SCHEME 1.** Synthesis of BODIPY 540 sphingosine.

comigrated with the analogous unlabeled sphingolipid in this solvent system, we identified the remaining fluorescent sphingolipid as BODIPY 540 glucosylceramide due to its comigration with the unlabeled standard. In addition to these four sphingolipid species, a fifth species, identified as lactosylceramide based on its relative location on the TLC plate (22), was observed for a labeling period of 1 day. More complex BODIPY 540-labeled glycosphingolipids, such as BODIPY 540 gangliosides, were not visible on the TLC plate (supplementary Fig. I). Because unlabeled gangliosides also were not detected on iodine-stained TLC plates, the inability to detect BODIPY 540 gangliosides likely reflects a low level of gangliosides in the NIH3T3 cell extracts and not a lack of BODIPY 540 sphingosine incorporation into complex glycosphingolipid species.

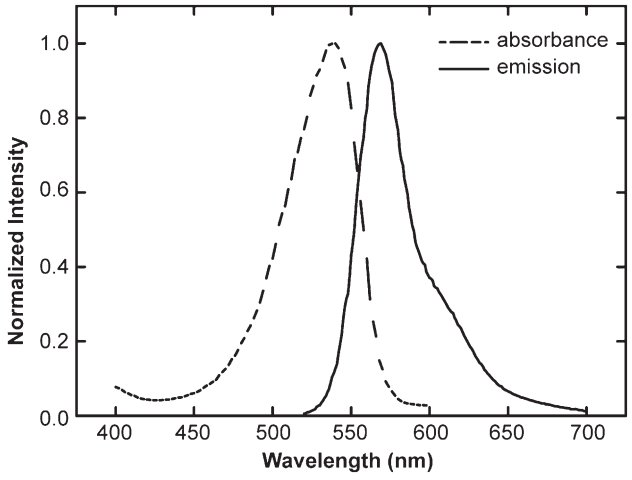


**Fig. 1.** Absorbance and emission spectra of BODIPY 540 sphingosine in ethanol. The emission spectrum was collected using 488 nm excitation.

Native sphingolipid catabolism yields phosphoethanolamine and the fatty aldehyde trans-2-hexadecenal, which is oxidized to a fatty acid that can be incorporated into glycerolipids (22–25). Therefore, if the BODIPY 540 sphingolipids were degraded via this pathway, the resulting BODIPY 540-labeled hexadecenal could be oxidized and used to biosynthesize fluorescent glycerolipids. To assess this possibility, sphingolipid extracts and total cellular lipid extracts were isolated from NIH3T3 cells that were cultured in the presence of 1 μM of BODIPY 540 sphingosine for 2 h, and the lipid components were separated with TLC. In addition to the BODIPY 540-labeled sphingolipid species observed by TLC separation of the sphingolipid extract, the total cellular lipid extract exhibited three additional fluorescent spots that corresponded to fluorescent glycerophospholipids (Fig. 2C). Comparison of these migration patterns to those of unlabeled

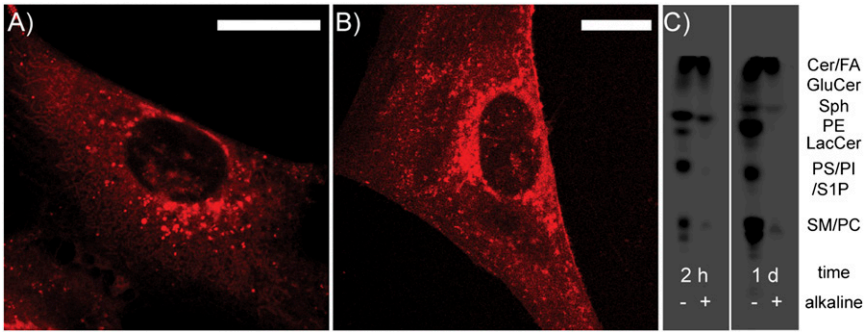


**Fig. 2.** Subcellular distribution and metabolism of BODIPY 540 sphingosine in NIH3T3 cells. Cells were incubated in 1.25 μM of BODIPY 540 sphingosine for 30 min followed by unlabeled medium for a chase time of 30 min (A) or 20 h (B). Bars = 20 μm. Although the plasma membrane of the cell shown in (B) is dim in comparison to the highly fluorescent intracellular vesicles that were especially abundant in the NIH3T3 cells we examined, the more distinct fluorescent outline at the edge of the cell indicates that BODIPY 540 lipids were present in the plasma membrane. C: Lipid fractions were isolated from cells that were labeled with BODIPY 540 sphingosine for 2 h or 1 day. The total lipid fractions (−) and the lipid fractions subjected to alkaline treatment to remove the glycerolipids (+) were separated by TLC, as described in the Materials and Methods. Images were taken on a fluorescence imager using 532 nm excitation and a 580 nm emission filter. The identities of the BODIPY 540-labeled species that are indicated to the right of each spot were determined by comparison to lipid standards (see Materials and Methods for details). Cer, ceramide; FA, fatty acids; GluCer, glucosylceramide; LacCer, lactosylceramide; PC, phosphatidylcholine; PE, phosphatidylethanolamine; PI, phosphatidylinositol; PS, phosphatidylserine; SM, sphingomyelin; Sph, sphingosine.

phospholipid standards indicated that two of these components were BODIPY 540-labeled phosphatidylcholine and phosphatidylethanolamine; the third spot was consistent with either BODIPY 540-labeled phosphatidylserine or phosphatidylinositol. Based on the relative intensities of the TLC spots corresponding to unlabeled lipid species, which were visualized by staining the same TLC plate with iodine, the BODIPY 540 fluorophore was incorporated into the major sphingolipid species but was less abundant in the major glycerolipid species after a 2 h labeling period (supplementary Fig. I). However, after labeling with 1 μM of BODIPY 540 sphingosine for 1 day, the BODIPY 540-labeled lipids reflected the major lipid species present in the cell extracts (supplementary Fig. I). These results suggest that fluorescent sphingolipid degradation followed the native sphingolipid catabolism pathway.

We estimated the fraction of BODIPY 540 that had been incorporated into glycerolipids after labeling NIH3T3 cells with 1 μM of BODIPY 540 sphingosine for 2 h and 1 day by measuring the fraction of the total fluorescence on the TLC plate that was produced by spots corresponding to glycerolipid species. After a 2 h labeling period, BODIPY 540 glycerolipids produced approximately 25% of the fluorescence measured in the total lipid extract; after labeling for 1 day, approximately 43% of the fluorescence measured in the total lipid extract was produced by BODIPY 540 glycerolipids. Thus, the BODIPY 540 glycerolipids that resulted from BODIPY 540 sphingolipid catabolism were detectable after a pulse as short as 2 h, and their abundance increased with time. Previous studies have demonstrated that exogenous [$^3$H] sphingosine is also rapidly degraded by cells and that the amount of the radioactive degradation products increases with time (26). This suggests that the time-dependent sphingolipid catabolism we observed is a characteristic of sphingosine pulse labeling and was not induced by the presence of the fluorophore.

### Subcellular distribution of BODIPY 540 sphingolipids

The studies described above demonstrate that NIH3T3 cells metabolized the BODIPY 540 sphingosine to fluorescent sphingolipids and degraded these fluorescent sphingolipids in a manner that was consistent with native sphingolipid catabolism. We performed colocalization studies to confirm that BODIPY 540 sphingosine and its fluorescent metabolites were trafficked through the organelles where sphingolipid biosynthesis primarily occurs. For these experiments, HEK293 cells were used because their high transfectability facilitated the expression of the organelle-specific fluorescent proteins required to assess colocalization. HEK293 cells that expressed the ER or Golgi apparatus markers, GFP-Sec61β (16) or CellLight™ Golgi-GFP, respectively, were pulse labeled with 1 μM of BODIPY 540 sphingosine for 30 min, followed by a 30 min or 1 day chase. Confocal microscopy imaging confirmed the fluorescent sphingolipid analogs were located in the ER (**Fig. 3A**) and Golgi apparatus (Fig. 3B) after the 30 min chase. Low colocalization occurred between the fluorescent sphingolipid analog and the ER or Golgi apparatus markers for the 1 day chase (Fig. 3C and 3D, respectively). The transient colocalization of the BODIPY 540 with the ER and Golgi apparatus is consistent with the conversion of BODIPY 540 sphingosine to more complex fluorescent sphingolipids in these organelles and the subsequent transport of the newly synthesized fluorescent sphingolipids to the plasma membrane (27).

Lysosomes are the subcellular compartment where complex sphingolipids are catabolized to sphingosine (28, 29), which can be reused for the biosynthesis of new

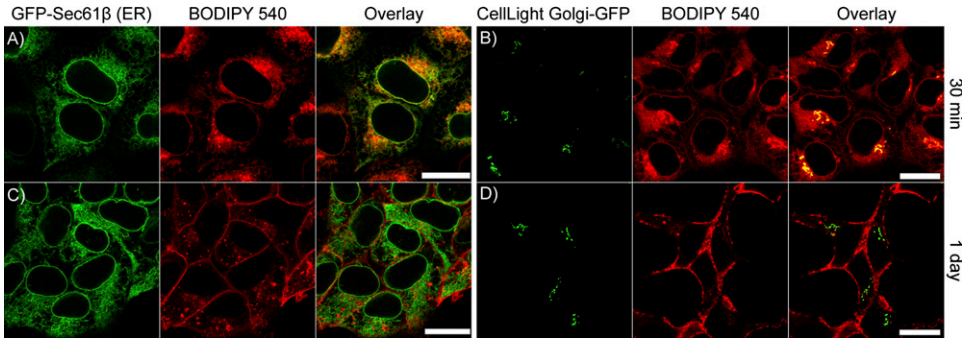


**Fig. 3.** Intracellular distribution of BODIPY 540 sphingosine and its fluorescent metabolites. Transfected HEK293 cells that expressed GFP-Sec61β or CellLight™-Golgi were pulse labeled for 30 min in medium containing 1 μM of BODIPY 540 sphingosine and transferred to unlabeled medium for the chase time indicated to the right of the last column. Confocal microscopy imaging was performed on living cells at room temperature. The GFP signal (green) locates the ER (A and C) or Golgi apparatus (B and D). The BODIPY 540 signal (red) shows the subcellular distribution of BODIPY 540 sphingosine and its fluorescent metabolites. The fluorescent outline of each cell, which signifies the incorporation of BODIPY 540 lipids into the plasma membrane, is especially distinct in these images because these HEK293 cells have few highly fluorescent intracellular vesicles. The overlay images show that colocalization between BODIPY 540 and each organelle-specific GPF fusion protein (yellow) occurred when the chase time was 30 min (A and B) but not 1 day (C and D). Bars = 20 μm.

sphingolipids, or degraded to nonsphingolipid species (23, 24, 30). We investigated whether BODIPY 540 sphingosine or its fluorescent metabolites accumulated in lysosomes by assessing colocalization between the lysosome marker, FITC-dextran (31), and BODIPY 540. NIH3T3 cells were labeled with FITC-dextran, pulse labeled for 30 min with BODIPY 540 sphingosine, and subjected to a 30 min or 16 h chase. Confocal microscopy imaging of these cells demonstrated that low levels of colocalization occurred after a 16 h chase time (**Fig. 4**). The lack of BODIPY 540 accumulation in the lysosomes confirms that the fluorescent sphingolipids that reached the lysosomes were promptly degraded, and the resulting fluorescent products were exported from the lysosomes.

Finally, we investigated whether BODIPY 540 sphingosine or its fluorescent metabolites could be detected in the mitochondria or nucleus. We focused on these organelles because sphingolipids and their metabolites have been previously detected within them, and the sphingolipid metabolism that occurs within these organelles plays a major role in modulating cellular function (2, 32–35). For example, internalized fluorescent ceramides are rapidly detected in mitochondria (35), where ceramide is catabolized to bioactive metabolites that promote the mitochondrial pathway of apoptosis (33). **Fig. 5A** demonstrates that the fluorescent sphingolipid analogs were colocalized with the mitochondria marker, CellLight™ mitochondria-GFP, in transfected HEK293 cells that were pulse labeled with BODIPY 540 sphingosine for 30 min and then chased for 30 min in unlabeled medium. Consistent with previous reports (35), colocalization was not observed after the 1 day chase. Sphingolipids also perform regulatory and structural functions in the nucleus, but their presence and distribution in subnuclear compartments have primarily been identified by biochemical analysis of nuclear extracts (2). To assess whether the BODIPY 540 sphingosine or its BODIPY 540-labeled metabolites could be detected in the nucleus, we performed colocalization studies between the DNA label, Hoechst 33342, and BODIPY 540 in labeled NIH3T3 cells. After labeling the DNA with Hoechst 33342, the cells were pulse labeled for 30 min with BODIPY 540 sphingosine, followed by a chase in unlabeled medium for approximately 2 days. From the en face confocal microscopy image acquired with the plane of focus at approximately the center of the cell (**Fig. 6A, D**), small amounts of the BODIPY 540

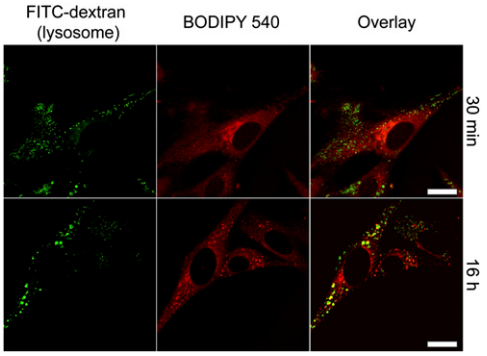


**Fig. 4.** Localization of BODIPY 540 sphingolipid analogs in lysosomes. The lysosomes in NIH3T3 cells were labeled by incubating the cells for 30 min in medium containing 2 mg/ml of FITC-dextran and then transferring the cells to label-free medium for 5 h. The lysosome-labeled NIH3T3 cells were incubated for 30 min in culture medium containing 1 μM of BODIPY 540 sphingosine and transferred to label-free medium for the chase time indicated to the right of the last column. Confocal imaging of the living cells at room temperature revealed the intracellular distribution of the FITC-dextran (green) that labeled the lysosomes and BODIPY 540 sphingosine and its metabolites (red). The overlay images (last column) show that colocalization between BODIPY 540 and FITC-dextran (yellow) did not occur after a 30 min chase but was detectable at low levels after a 16 h chase. Bars = 20 μm.

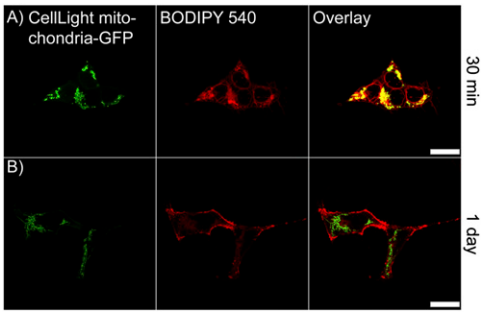


**Fig. 5.** Transfected HEK293 cells that expressed CellLight™ mitochondria-GFP were pulse labeled for 30 min in medium containing 1 μM of BODIPY 540 sphingosine and transferred to unlabeled medium for 30 min (A) or 1 day (B). The locations of the mitochondria (green) and BODIPY 540 sphingolipid analogs (red) were imaged in living cells at room temperature with confocal microscopy. The overlay images (last column) show that a high amount of colocalization occurred between BODIPY 540 and CellLight™ mitochondria-GFP (yellow) 30 min after pulse labeling. In contrast, colocalization of the two fluorescent components was not detected when the chase time increased to 1 day. Bars = 20 μm.

fluorophore appeared to be in close proximity to a DNA segment in the nucleus. The reconstructed cross-sectional z-stack images acquired along (Fig. 6B, E) and perpendicular to (Fig. 6C, F) the DNA segment also indicate that the BODIPY 540 fluorophore was inside the nucleus and adjacent to the DNA segment. Based on the previously reported finding that sphingomyelin is associated with chromatin (36), the BODIPY 540-labeled molecule associated with the DNA segment is likely BODIPY 540 sphingomyelin. To our knowledge, this is the first time that a fluorescent sphingolipid has been detected in the nucleus of a living cell.

## DISCUSSION

We have described the synthesis of a new fluorescent sphingosine analog, BODIPY 540 sphingosine, and verified its efficacy for studying the transport, distribution, and metabolism of sphingolipids within living cells. BODIPY 540 sphingosine enabled imaging unacylated sphingolipids, which cannot be accomplished with the existing sphingolipid analogs that contain a fluorescent fatty acid side chain. Furthermore, unlike previously reported fluorescent sphingosine analogs (7–9), BODIPY 540 sphingosine can be visualized in parallel with GFP without the use of UV excitation. By exploiting these capabilities, we verified that mammalian cells rapidly internalized BODIPY 540 sphingosine, transported it to the secretory pathway where it was metabolized to more complex fluorescent sphingolipids, and eventually catabolized these fluorescent sphingolipids. The similarity in the pattern of BODIPY 540 sphingosine metabolites and their subcellular distribution to those of the native sphingolipids indicates that the fluorophore did not significantly hinder lipid metabolism or trafficking.

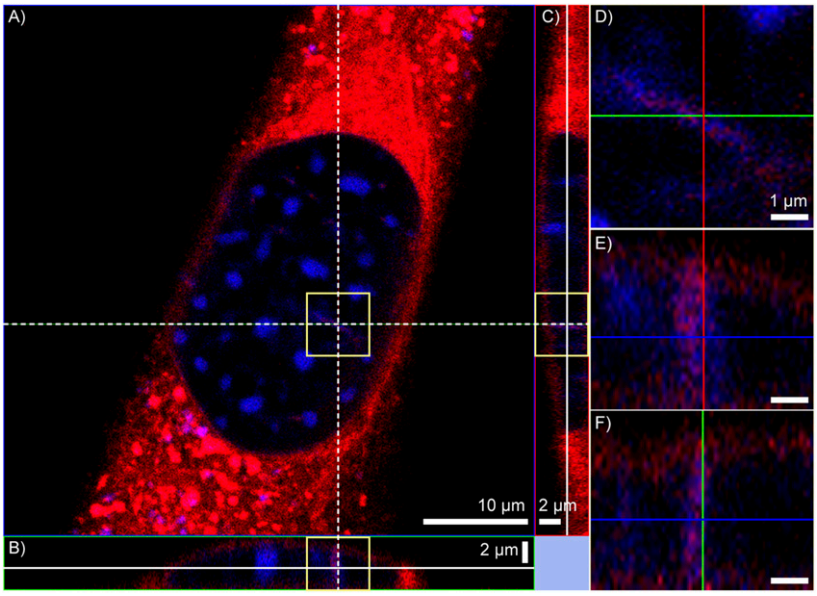


**Fig. 6.** The DNA in NIH3T3 cells was labeled with Hoechst 33342 for 30 min. After 30 min in unlabeled medium, the cells were pulse labeled for 30 min with BODIPY 540 sphingosine and chased in unlabeled medium for approximately 2 days. Confocal imaging of the cell shows the subcellular location of DNA (blue) and BODIPY 540 sphingolipid analogs (red). A: An en face confocal microscopy image acquired with the plane of focus at approximately the center of the cell. The horizontal and vertical white dashed lines denote where cross-sectional images were acquired. B: Reconstructed cross-section acquired at the vertical white dashed line shown in A. Z-scan step: 0.2 μm. C: Reconstructed cross-section acquired at the horizontal white dashed line shown in A. Z-scan step: 0.2 μm. D: Enlargement of the region outlined in yellow in A. E: Enlargement of the region outlined in yellow in B. F: Enlargement of the region outlined in yellow in C. Bars in E and F = 1 μm.

Our finding that BODIPY 540 sphingosine and its metabolites mimicked the analogous native species in living cells is advantageous for using this probe to study dynamic sphingolipid processes but also has implications for its usage. Sphingosine is a bioactive signaling molecule, so consideration must be given to the biological effects that may be induced by labeling with the fluorescent analog. The BODIPY 540 sphingosine concentrations used in this work were substantially higher than the sphingosine concentrations found in human or bovine serum (~20 nM) (37, 38). However, NIH3T3 cells did not exhibit the changes in morphology or growth rate that are characteristic of sphingosine toxicity during or after BODIPY 540 sphingosine labeling (39). HEK293 cells were more sensitive to the exogenous sphingosine analog; changes in their morphology occurred during pulse labeling but subsided shortly after transfer to unlabeled chase medium. Previous reports have shown that the effects of exogenous sphingosine depend on the dose per cell and the cell's capacity to metabolize it (39), so the adverse effects of labeling sensitive cell lines might be reduced by decreasing the BODIPY 540 sphingosine concentration. Alternatively, for labeling more sensitive cell lines, BODIPY 540 sphingosine may need to be synthetically converted to BODIPY 540 sphingomyelin (40, 41), which would have lower bioactivity (1) and permit visualizing acylated and unacylated sphingolipids in parallel with GFP.

The cells' capacity to degrade the BODIPY 540 sphingolipids in a manner consistent with the native sphingolipid catabolism pathway, which resulted in fluorophore incorporation into glycerolipid species, including phosphatidylcholine, phosphatidylethanolamine, and either phosphatidylserine or phosphatidylinositol, also has implications for use of BODIPY 540 sphingosine. This property permits observing the entire sphingolipid catabolism pathway, which could shed light on the cellular mechanisms that underlie sphingolipid homeostasis. However, this catabolism complicates using BODIPY 540 sphingosine to visualize the subcellular sphingolipid distribution because some of the fluorescence observed will be produced by glycerolipids. The same problem is encountered with fluorescent sphingolipid analogs that contain a fluorophore-labeled *N*-acyl fatty acid because they are also catabolized to fluorescent fatty acids that are incorporated into glycerolipids (5). We observed that the incorporation of BODIPY 540 into glycerolipids increased with increasing labeling time, so the fluorescence from nonsphingolipid species can be minimized by limiting the labeling time. In addition, the irreversible degradation of sphingosine-1-phosphate to fatty acid precursors, which causes the label scrambling we observed, has been shown to increase with increasing sphingosine concentration in the medium (26, 39). Thus, decreasing the BODIPY 540 sphingosine concentration in the labeling media should reduce fluorophore incorporation into glycerolipid species.

The ability to track unacylated sphingolipid analogs with BODIPY 540 sphingosine opens the door to identifying the subcellular locations where these bioactive molecules encounter their targets. One such unacylated sphingolipid, sphingosine-1-phosphate, stimulates signaling by binding to G protein-coupled receptors on the cell surface (1, 24). Recently, the hypothesis that fundamental cellular processes are regulated by sphingosine-1-phosphate binding to intracellular targets was verified. Specifically, sphingosine-1-phosphate binding to histone deacetylases in the nucleus regulates gene transcription (34), whereas its binding to the proapoptotic effector molecule, BAK, in mitochondria promotes apoptosis (33). In both cases, the sphingosine-1-phosphate was generated in the organelle where its target resided, and this location determined the effects of this binding on cell function. Efforts to identify additional intracellular targets of unacylated sphingolipids and their mechanisms of action may be facilitated by visualizing the subcellular distributions of BODIPY 540 sphingosine metabolites and GFP-labeled sphingolipid metabolizing enzymes in parallel.

The detection of BODIPY 540 sphingosine metabolites associated with DNA in the nucleus demonstrates the potential to discover new phenomena by metabolic labeling with BODIPY 540 sphingosine. To our knowledge, this is the first observation of fluorescent sphingosine metabolite association with DNA in the nucleus of a living cell, although further studies are required to confirm the BODIPY 540-labeled molecule was BODIPY 540 sphingomyelin. Since their detection in the nucleus decades ago (42, 43), the identities and subnuclear distributions of sphingolipids have been primarily probed by biochemical analysis of isolated nuclei and visualization of sphingolipid-specific functionalized affinity labels (2, 44, 45). Additionally, structural and regulatory roles performed by various types of sphingolipids in the nucleus have been identified (2). Sphingomyelin associates with chromatin and stabilizes DNA and newly synthesized RNA (45, 46), GM1 regulates nuclear calcium concentrations (44), and nuclear ceramide is involved in proliferation and apoptosis, although the precise mechanisms remain to be established (47–49). As mentioned above, nuclear sphingosine-1-phosphate regulates gene expression by binding to histone deacetylases, thereby inhibiting histone deacetylation (34). Despite these discoveries, many aspects of nuclear sphingolipid function remain poorly understood. BODIPY 540 sphingosine may potentially be used to visualize nuclear sphingolipids, which may allow for a better understanding of how various stimuli influence nuclear sphingolipid distribution and the consequences for cell function.

BODIPY 540 sphingosine can be used to monitor the trafficking and metabolism of acylated and unacylated sphingolipids in living cells. Assessment of colocalization between BODIPY 540 sphingolipids and with GFP-labeled proteins of interest will facilitate identifying the subcellular locations where sphingolipids are metabolized or encounter their binding targets. Such studies can provide new insight into the broad roles of sphingolipids in modulating cellular function.

The authors thank Lauren Macur Brousil for her assistance with the TLC separation and Prof. Hyunjoon Kong and Steven Caliari at the University of Illinois for their discussions of the Hoechst 33342 data.

## REFERENCES


1. Hannun, Y. A., and L. M. Obeid. 2008. Principles of bioactive lipid signalling: lessons from sphingolipids. *Nat. Rev. Mol. Cell Biol.* **9:** 139–150.
2. Lucki, N. C., and M. B. Sewer. 2012. Nuclear sphingolipid metabolism. *Annu. Rev. Physiol.* **74:** 131–151.
3. Kolter, T. 2011. A view on sphingolipids and disease. *Chem. Phys. Lipids.* **164:** 590–606.
4. Kolter, T., and K. Sandhoff. 2006. Sphingolipid metabolism diseases. *Biochim. Biophys. Acta.* **1758:** 2057–2079.
5. Rasmussen, J-A. M., and A. Hermetter. 2008. Chemical synthesis of fluorescent glycero- and sphingolipids. *Prog. Lipid Res.* **47:** 436–460.
6. Kuerschner, L., C. S. Ejsing, K. Ekroos, A. Shevchenko, K. I. Anderson, and C. Thiele. 2005. Polyene-lipids: a new tool to image lipids. *Nat. Methods.* **2:** 39–45.
7. Ettmayer, P., A. Billich, T. Baumruker, D. Mechtcheriakova, H. Schmid, and P. Nussbaumer. 2004. Fluorescence-labeled sphingosines as substrates of sphingosine kinases 1 and 2. *Bioorg. Med. Chem. Lett.* **14:** 1555–1558.
8. Peters, C., A. Billich, M. Ghobrial, K. Hoegenauer, T. Ullrich, and P. Nussbaumer. 2007. Synthesis of borondipyrromethene (BODIPY)-labeled sphingosine derivatives by cross-metathesis reaction. *J. Org. Chem.* **72:** 1842–1845.
9. Hakogi, T., T. Shigenari, S. Katsumura, T. Sano, T. Kohno, and Y. Igarashi. 2003. Synthesis of fluorescence-labeled sphingosine and sphingosine 1-phosphate; effective tools for sphingosine and sphingosine 1-phosphate behavior. *Bioorg. Med. Chem. Lett.* **13:** 661–664.
10. Bode, C., S-C. Sensken, U. Peest, G. Beutel, F. Thol, B. Levkau, Z. Li, R. Bittman, T. Huang, M. Tölle, et al. 2010. Erythrocytes serve as a reservoir for cellular and extracellular sphingosine 1-phosphate. *J. Cell. Biochem.* **109:** 1232–1243.
11. Snapp, E. L. 2009. Fluorescent proteins: a cell biologist's user guide. *Trends Cell Biol.* **19:** 649–655.
12. Alexandrova, L. A., M. V. Jasko, E. E. Belobritskaya, A. V. Chudinov, O. N. Mityaeva, T. V. Nasedkina, A. S. Zasedatelev, and M. K. Kukhanova. 2007. New triphosphate conjugates bearing reporter groups: labeling of DNA fragments for microarray analysis. *Bioconjug. Chem.* **18:** 886–893.
13. Coleman, R. S., and A. J. Carpenter. 1992. Diastereoselective addition of vinyl organometallic reagents to L-serinal. *Tetrahedron Lett.* **33:** 1697–1700.
14. Nussbaumer, P., P. Ettmayer, C. Peters, D. Rosenbeiger, and K. Hogenauer. 2005. One-step labelling of sphingolipids via a scrambling cross-metathesis reaction. *Chem. Commun. (Camb.).* **40:** 5086–5087.
15. Bligh, E. G., and Dyer, W. J. 1959. A rapid method of total lipid extraction and purification. *Can. J. Biochem. Physiol.* **37:** 911–917.
16. Voeltz, G. K., W. A. Prinz, Y. Shibata, J. M. Rist, and T. A. Rapoport. 2006. A class of membrane proteins shaping the tubular endoplasmic reticulum. *Cell.* **124:** 573–586.
17. Johnson, I. D., H. C. Kang, and R. P. Haugland. 1991. Fluorescent membrane probes incorporating dipyrromethene boron difluoride fluorophores. *Anal. Biochem.* **198:** 228–237.
18. Boldyrev, I. A., X. Zhai, M. M. Momsen, H. L. Brockman, R. E. Brown, and J. G. Molotkovsky. 2007. New BODIPY lipid probes for fluorescence studies of membranes. *J. Lipid Res.* **48:** 1518–1532.
19. Eggers, F., and U. Luening. 2009. Concave 1,10-phenanthrolines as ligands for cyclopropanations: towards a deeper understanding of the stereoselectivity. *Eur. J. Org. Chem.* **2009:** 2328–2341.
20. Lee, P. H. 2008. Synthesis of 4,4-difluoro-4-bora-3a,4a-diaza-s-indacene dyes bearing new aryl substituents at C3- and C5-positions. *Bull. Korean Chem. Soc.* **29:** 261–264.
21. Sullards, M. C., and A. H. Merrill, Jr. 2001. Analysis of sphingosine 1-phosphate, ceramides, and other bioactive sphingolipids by high-performance liquid chromatography-tandem mass spectrometry. *Sci. STKE.* **2001:** pl1.
22. Nakahara, K., A. Ohkuni, T. Kitamura, K. Abe, T. Naganuma, Y. Ohno, R. A. Zoeller, and A. Kihara. 2012. The Sjögren-Larsson syndrome gene encodes a hexadecenal dehydrogenase of the sphingosine 1-phosphate degradation pathway. *Mol. Cell.* **46:** 461–471.
23. Van Veldhoven, P. P., and G. P. Mannaerts. 1991. Subcellular localization and membrane topology of sphingosine-1-phosphate lyase in rat liver. *J. Biol. Chem.* **266:** 12502–12507.
24. Maceyka, M., S. Milstien, and S. Spiegel. 2009. Sphingosine-1-phosphate: the Swiss army knife of sphingolipid signaling. *J. Lipid Res.* **50:** S272–S276.
25. Stoffel, W., and G. Sticht. 1967. Metabolism of sphingosine bases, II. Studies on the degradation and transformation of [3-$^{14}$C] *erythro*-DL-dihydrosphingosine, [7-$^{3}$H] *erythro*-DL-sphingosine, [5-$^{3}$H] *threo*-L-dihydrosphingosine and [3-$^{14}$C;1-$^{3}$H] *erythro*-DL-dihydrosphingosine in rat liver. *Hoppe Seylers Z. Physiol. Chem.* **348:** 1345–1351.
26. Riboni, L., R. Bassi, A. Prinetti, P. Viani, and G. Tettamanti. 1999. Predominance of the acylation route in the metabolic processing of exogenous sphingosine in neural and extraneural cells in culture. *Biochem. J.* **338:** 147–151.
27. Bartke, N., and Y. A. Hannun. 2009. Bioactive sphingolipids: metabolism and function. *J. Lipid Res.* **50:** S91–S96.
28. Kolter, T., and K. Sandhoff. 2010. Lysosomal degradation of membrane lipids. *FEBS Lett.* **584:** 1700–1712.
29. Schulze, H., T. Kolter, and K. Sandhoff. 2009. Principles of lysosomal membrane degradation: cellular topology and biochemistry of lysosomal lipid degradation. *Biochim. Biophys. Acta Cell Res.* **1793:** 674–683.
30. Kitatani, K., J. Idkowiak-Baldys, and Y. A. Hannun. 2008. The sphingolipid salvage pathway in ceramide metabolism and signaling. *Cell. Signal.* **20:** 1010–1018.
31. Schmid, S. L., R. Fuchs, P. Male, and I. Mellman. 1988. Two distinct subpopulations of endosomes involved in membrane recycling and transport to lysosomes. *Cell.* **52:** 73–83.
32. Ardail, D., I. Popa, K. Alcantara, A. Pons, J. P. Zanetta, P. Louisot, L. Thomas, and J. Portoukalian. 2001. Occurrence of ceramides and neutral glycolipids with unusual long-chain base composition in purified rat liver mitochondria. *FEBS Lett.* **488:** 160–164.
33. Chipuk, J. E., G. P. McStay, A. Bharti, T. Kuwana, C. J. Clarke, L. J. Siskind, L. M. Obeid, and D. R. Green. 2012. Sphingolipid metabolism cooperates with BAK and BAX to promote the mitochondrial pathway of apoptosis. *Cell.* **148:** 988–1000.
34. Hait, N. C., J. Allegood, M. Maceyka, G. M. Strub, K. B. Harikumar, S. K. Singh, C. Luo, R. Marmorstein, T. Kordula, S. Milstien, et al. 2009. Regulation of histone acetylation in the nucleus by sphingosine-1-phosphate. *Science.* **325:** 1254–1257.
35. Lipsky, N. G., and R. E. Pagano. 1985. Intracellular translocation of fluorescent sphingolipids in cultured fibroblasts: endogenously synthesized sphingomyelin and glucocerebroside analogues pass through the Golgi apparatus en route to the plasma membrane. *J. Cell Biol.* **100:** 27–34.
36. Scassellati, C., E. Albi, D. Cmarko, C. Tiberi, J. Cmarkova, C. Bouchet-Marquis, P. J. Verschure, R. van Driel, M. V. Magni, and S. Fakan. 2010. Intranuclear sphingomyelin is associated with transcriptionally active chromatin and plays a role in nuclear integrity. *Biol. Cell.* **102:** 361–375.
37. Ribar, S., M. Mesaric, and M. Bauman. 2001. High-performance liquid chromatographic determination of sphinganine and sphingosine in serum and urine of subjects from an endemic nephropathy area in Croatia. *J. Chromatogr. B Biomed. Sci. Appl.* **754:** 511–519.
38. Mathur, S., P. D. Constable, R. M. Eppley, M. E. Tumbleson, G. W. Smith, W. J. Tranquilli, D. E. Morin, and W. M. Haschek. 2001. Fumonisin B1 increases serum sphinganine concentration but does not alter serum sphingosine concentration or induce cardiovascular changes in milk-fed calves. *Toxicol. Sci.* **60:** 379–384.
39. Riboni, L., A. Prinetti, R. Bassi, P. Viani, and G. Tettamanti. 1998. The effects of exogenous sphingosine on Neuro2a cells are strictly related to the overall capacity of cells to metabolize sphingosine. *J. Biochem.* **124:** 900–904.
40. Ahmad, T. Y., J. T. Sparrow, and J. D. Morrisett. 1985. Fluorine-, pyrene-, and nitroxide-labeled sphingomyelin: semi-synthesis and thermotropic properties. *J. Lipid Res.* **26:** 1160–1165.
41. Byun, H-S., R. K. Erukulla, and R. Bittman. 1994. Synthesis of sphingomyelin and ceramide 1-phosphate from ceramide without protection of the allylic hydroxyl group. *J. Org. Chem.* **59:** 6495–6498.
42. Manzoli, F. A., N. M. Maraldi, L. Cocco, S. Capitani, and A. Facchini. 1977. Chromatin phospholipids in normal and chronic lymphocytic leukemia lymphocytes. *Cancer Res.* **37:** 843–849.
43. Cocco, L., N. M. Maraldi, F. A. Manzoli, R. Stewart Gilmour, and A. Lang. 1980. Phospholipid interactions in rat liver nuclear matrix. *Biochem. Biophys. Res. Commun.* **96:** 890–898.

44. Ledeen, R. W., and G. Wu. 2006. Gangliosides of the nuclear membrane: a crucial locus of cytoprotective modulation. *J. Cell. Biochem.* **97:** 893–903.
45. Albi, E., and M. P. Viola Magni. 2004. The role of intranuclear lipids. *Biol. Cell.* **96:** 657–667.
46. Micheli, M., E. Albi, C. Leray, and M. V. Magni. 1998. Nuclear sphingomyelin protects RNA from RNase action. *FEBS Lett.* **431:** 443–447.
47. Albi, E., S. Cataldi, G. Rossi, M. Viola Magni, M. Toller, S. Casani, and G. Perrella. 2008. The nuclear ceramide/diacylglycerol balance depends on the physiological state of thyroid cells and changes during UV-C radiation-induced apoptosis. *Arch. Biochem. Biophys.* **478:** 52–58.
48. Watanabe, M., T. Kitano, T. Kondo, T. Yabu, Y. Taguchi, M. Tashima, H. Umehara, N. Domae, T. Uchiyama, and T. Okazaki. 2004. Increase of nuclear ceramide through caspase-3-dependent regulation of the "sphingomyelin cycle" in Fas-induced apoptosis. *Cancer Res.* **64:** 1000–1007.
49. Tsugane, K., K. Tamiya-Koizumi, M. Nagino, Y. Nimura, and S. Yoshida. 1999. A possible role of nuclear ceramide and sphingosine in hepatocyte apoptosis in rat liver. *J. Hepatol.* **31:** 8–17.